Research article

LUMINESCENCE
The Journal of Biological and Chemical Luminescence

Received: 24 December 2013, Revised: 10 April 2014, Accepted: 22 May 2014 Published online in Wiley Online Library

(wileyonlinelibrary.com) DOI 10.1002/bio.2725

Study on the synthesis of sulfonamide derivatives and their interaction with bovine serum albumin

Xuehong Zhang,[a,b] Yijie Lin,[a] Lina Liu[a] and Cuiwu Lin[a]*

ABSTRACT: Three sulfonamide derivatives (SAD) were first synthesized from *p*-hydroxybenzoic acid and sulfonamides (sulfadimidine, sulfamethoxazole and sulfachloropyridazine sodium) and were characterized by elemental analysis, ^{1}H NMR and MS. The interaction between bovine serum albumin (BSA) and SAD was studied using UV/vis absorption spectroscopy, fluorescence spectroscopy, time-resolved fluorescence spectroscopy and circular dichroism spectra under imitated physiological conditions. The experimental results indicated that SAD effectively quenched the intrinsic fluorescence of BSA via a static quenching process. The thermodynamic parameters showed that hydrogen bonding and van der Waal's forces were the predominant intermolecular forces between BSA and two SADs [4-((4-(*N*-(4,6-dimethylpyrimidin-2-yl)sulfamoyl)phenyl)carbamoyl)phenyl acetate and 4-((4-(*N*-(5-methylisoxazol-3-yl)sulfamoyl)phenyl)carbamoyl)phenyl acetate], but hydrophobic forces played a major role in the binding process of BSA and 4-((4-(*N*-(6-chloropyridazin-3-yl)sulfamoyl)phenyl) carbamoyl)phenyl acetate. In addition, the effect of SAD on the conformation of BSA was investigated using synchronous fluorescence spectroscopy and circular dichroism spectra. Molecular modeling results showed that SAD was situated in subdomain IIA of BSA. Copyright © 2014 John Wiley & Sons, Ltd.

Keywords: synthesis; sulfonamide derivatives; bovine serum albumin

Introduction

Serum albumin (SA) is the most abundant protein in the circulatory system and contributes ~80% of the osmotic pressure of blood (1); it is also responsible for the maintenance of blood pH (2). It can transport many endogenous and exogenous substances, such as fatty acids, amino acids, steroids, metal ions and drugs, and modulate their delivery to cells *in vitro* and *in vivo* (3,4). The binding ability of a drug to the SA will affect its absorption, distribution and metabolism in blood (5,6). Therefore, research on the interaction between drugs and proteins has important theoretical and practical significance in biochemistry and biomedicine. In this study, bovine serum albumin (BSA) was selected as a model protein to study drug–protein interactions because of its low cost, ready availability and unusual ligand-binding properties. What is more, BSA has been proven to have a high homology and similarities in sequence and conformation with human serum albumin (HSA) (7,8).

Sulfonamides are an important class of drugs, possessing various types of pharmacological activities such as antibacterial, anticarbonic anhydrase, high-ceiling diuretic, hypoglycemic, antithyroid, anti-inflammatory and antiglaucoma (9). They are commonly used in human and veterinary medicine for therapeutic and prophylactic purposes to fight common bacterial diseases (10). However, sulfonamides have more adverse reactions including nephrotoxicity (11), and so chemical modification of sulfonamides is necessary.

Phenolic compounds are reported to have multiple biological effects, including antioxidant activity (12), antitumor (13), antimutagenic (14), and antibacterial and angioprotective properties (15). This group of compounds includes hydroxybenzoic acid. *p*-Hydroxybenzoic acid is used in the preparation of biocides, antiseptics and bacteriostatic agents; at the same time, it is also used as a chemical intermediate in drug synthesis.

Some reports on the synthesis and physiological activity of sulfonamide derivatives (SADs) have been published (16–18), but the synthesis of sulfonamide derivatives using *p*-hydroxybenzoic acid as a raw material, and the interaction between sulfonamide derivatives and BSA or HSA have not been reported to date. Here, three SADs were synthesized from sulfonamides and *p*-hydroxybenzoic acid, and were characterized by elemental analysis, ^{1}H NMR and MS. The interaction between BSA and SAD was investigated under physiological conditions by UV/vis absorption spectra, fluorescence quenching spectra, time-resolved fluorescence spectroscopy and circular dichroism (CD) spectra.

Experimental

Reagents

BSA was purchased from Biological Technology Co. (Shanghai, China) and was dissolved in doubly distilled water to prepare a stock solution of 1.00×10^{-4} mol/L. *p*-Hydroxybenzoic acid, sulfadimidine, sulfamethoxazole and sulfachloropyridazine sodium

* Correspondence to: C. Lin, College of Chemistry and Chemical Engineering, Guangxi University, Nanning, 530004, China. E-mail: cuiwulin@163.com

[a] College of Chemistry and Chemical Engineering, Guangxi University, Nanning, 530004, China

[b] School of Chemistry and Life Science, Guangxi Teachers Education University, Nanning, 530001, China

were obtained from Sinopharm Group Chemical Reagent Co., Ltd. (Shanghai, China). SAD stock solutions (1.0×10^{-4} mol/L) were prepared by dissolving SAD in 20% dimethyl sulfoxide (DMSO) Tris/HCl buffer solution. Tris/HCl buffer (0.05 mol/L, pH 7.40) containing 0.10 mol/L NaCl was selected to keep the pH value constant and to maintain the ionic strength of the solution. All reagents were of analytical reagent grade and were used without further purification.

Apparatus and methods

UV/vis absorption spectra were performed on a Varian Cary 50 UV/vis spectrophotometer at room temperature. The absorption spectra of BSA in the presence of SAD were recorded in the 200–400 nm region. The concentration of BSA was 1.0×10^{-5} mol/L and that of SAD was varied from 0 to 2.00×10^{-5} mol/L in steps of 5.0×10^{-6} mol/L. In addition, the absorption spectra of SAD at 1.00×10^{-5} mol/L were measured over the range 200–400 nm.

Fluorescence spectra were recorded on a Shimadzu RF-5301PC spectrofluorometer equipped with a xenon lamp source and a 1.0 cm quartz cell. Fluorescence quenching spectra were measured over the range 300–450 nm with an excitation wavelength of 295 nm at five temperatures (298, 301, 304, 307 and 310 K). Synchronous fluorescence spectra were obtained by setting the excitation and emission wavelength intervals, $\Delta\lambda$, at 15 and 60 nm. The widths of the excitation and emission slits were set to 3.0 nm.

Fluorescence lifetime was measured using the time-correlated single-photon counting (TCSPC) method with a Horiba Jobin Yvon Fluorocube at room temperature. The sample was excited at 280 nm using a pulsed diode Nano LED-280 as light source. The average fluorescence lifetime (τ_f) was calculated as (19):

$$\tau_f = \frac{\sum_i a_i \tau_i^2}{\sum_i a_i \tau_i} \quad (1)$$

where a_i and τ_i denote the pre-exponential factor and the corresponding lifetime, respectively.

CD spectra were recorded by a Bio-Logic CD spectrometer, model MOS-450, using a 0.1 cm path length quartz cell and a wavelength range between 200 and 260 nm. Elemental analysis was carried out on a Perkin–Elmer 2400 elemental analyser. ^{1}H NMR spectra were recorded on a Bruker Advance III 300 NMR spectrometer in DMSO-d_6 solution with TMS as the internal standard. The mass spectrum was recorded using a Thermo LCQ DECA XP LC-MS spectrometer.

Synthesis

***p*-Acetoxybenzoic acid.** *p*-Hydroxybenzoic acid (10 g, 72 mmol) and acetic anhydride (50 mL) were introduced into a three-necked flask with a magnetic stirrer and a reflux condenser. The mixture was heated in an oil bath and stirred at 385 K for 4 h. The reaction mixture was then diluted with water (500 mL), filtered, washed repeatedly with water and dried to obtain 11.7 g of *p*-acetoxybenzoic acid (white solid).

***p*-Acetoxy benzoyl chloride.** *p*-Acetoxybenzoic acid (10 g, 55 mmol) and thionyl chloride (40 mL) were introduced into a three-necked flask with a magnetic stirrer and a reflux condenser. The mixture was heated in an oil bath and stirred at 355 K for 5 h. The resulting mixture was then distilled under reduced pressure to remove the thionyl chloride. Finally, a pale yellow oily liquid was obtained, which is *p*-acetoxy benzoyl chloride.

Sulfonamide derivatives. Sulfonamide (56 mmol) and pyridine (5 mL) were added to a solution of *p*-acetoxy benzoyl chloride in tetrahydrofuran at 275 K, and the mixture was stirred at the same temperature for 1.5 h and at room temperature for 24 h. The crude product was isolated by filtration after adding water, washed repeatedly with water (1 L), dried and recrystallized from methanol–tetrahydrofuran to obtain a pure sulfonamide derivative. The chemical structures of three sulfonamide derivatives are listed in Scheme 1.

4-((4-(*N*-(4,6-dimethylpyrimidin-2-yl)sulfamoyl)phenyl)carbamoyl) phenyl acetate (DOPS). DOPS has the following properties: white powder, yield: 78%, mp: 248–249 °C. Anal. calcd (%) for $C_{21}H_{20}N_4O_5S$: C, 57.26; H, 4.58; N, 12.72. Found (%): C, 57.73; H, 4.11; N, 12.83. MS (*m/z*): 400.2. Calcd. 400.08. ^{1}H NMR (300 MHz, DMSO): δ (ppm): 2.264 (s, 6H, -CH_3); 2.311 (s, 3H, -CH_3-CO); 6.767 (s,1H, Py-H); 7.288–7.304 (t, 1H, Ar-H, *J* = 1.6 Hz); 7.320–7.335 (t, 1H, Ar-H, *J* = 1.5 Hz); 7.918–7.948 (d, 2H, Ar-H, *J* = 4.5 Hz); 7.973–8.003 (m, 3H); 8.011–8.027 (t, 1H, Ar-H, *J* = 1.6 Hz); 10.586 (s, 1H, -CO-NH); 11.621 (s, 1H, -SO_2-NH).

4-((4-(*N*-(5-methylisoxazol-3-yl)sulfamoyl)phenyl)carbamoyl)phenyl acetate (MIOS). MIOS has the following properties: white powder, yield: 73%, mp: 264–266 °C. Anal. calcd (%) for $C_{19}H_{17}N_3O_6S$: C, 54.93; H, 4.12; N, 10.12. Found (%): C, 55.15; H, 4.06; N, 10.03. MS (*m/z*): 415.1. Calcd. 415.08. ^{1}H NMR (300 MHz, DMSO), δ (ppm): 2.303–2.305 (d, 3H, -CH_3-CO, *J* = 0.3 Hz); 2.313 (s, 3H, -CH3); 6.147–6.150 (d,1H, isoxazole-H, *J* = 0.45 Hz); 7.297–7.312 (t, 1H, Ar-H, *J* = 1.5 Hz); 7.328–7.343 (t, 1H, Ar-H, *J* = 1.5 Hz); 7.825–7.839 (t, 1H, Ar-H, *J* = 1.4 Hz); 7.856–7.870 (t, 1H, Ar-H, *J* = 1.4 Hz); 7.957–7.971 (t, 1H, Ar-H, *J* = 1.4 Hz); 7.987–7.994 (d, 2H, Ar-H , *J* = 1.05 Hz); 8.009–8.025 (t, 1H, Ar-H, *J* = 1.6 Hz); 10.654 (s,1H, -CO-NH); 11.365 (s,1H, -SO_2-NH).

4-((4-(*N*-(6-chloropyridazin-3-yl)sulfamoyl)phenyl)carbamoyl)phenyl acetate (CPDS). CPDS has the following properties: pale yellow powder, yield: 76%, mp: 239–240 °C. Anal. calcd (%) for $C_{19}H_{15}ClN_4O_5S$: C, 51.07; H, 3.38; N, 12.54. Found (%): C, 50.87; H, 3.26; N, 12.41. MS (*m/z*): 447.1. Calcd. 446.05. ^{1}H NMR (300 MHz, DMSO), δ (ppm): 2.311 (s, 3H, -CH3); 7.293–7.308

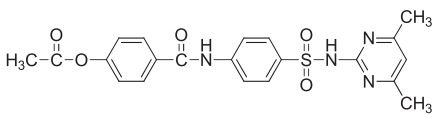

4-((4-(*N*-(4,6-dimethylpyrimidin-2-yl)sulfamoyl)phenyl)carbamoyl)phenyl acetate

DOPS

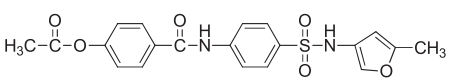

4-((4-(*N*-(5-methylfuran-3-yl)sulfamoyl)phenyl)carbamoyl)phenyl acetate

MIOS

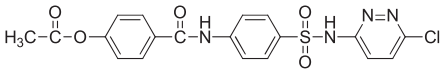

4-((4-(*N*-(6-chloropyridazin-3-yl)sulfamoyl)phenyl)carbamoyl)phenyl acetate

CPDS

Scheme 1. The structures of three sulfonamide derivatives.

LUMINESCENCE
The Journal of Biological and Chemical Luminescence

(t,1H, chloropyridazine-H, $J = 1.5$ Hz); 7.324–7.339 (t, 1H, chloropyridazine-H, $J = 1.5$ Hz); 7.578 (s, 1H, Ar-H); 7.771–7.803 (d, 1H, Ar-H, $J = 4.8$ Hz); 7.899–7.929 (d, 2H, Ar-H, $J = 4.5$ Hz); 7.964–7.986 (d, 3H, Ar-H, $J = 4.5$ Hz); 8.009–8.015 (d, 1H, Ar-H, $J = 0.9$ Hz); 10.636 (s, 1H, -CO-NH); 11.925 (s, 1H, -SO_2-NH).

Molecular docking

To obtain the binding energy of BSA–SAD complex and identify the potential binding sites, molecular docking simulation was performed using the software package AutoDock 4.2 (20), in which the Lamarckian Genetic Algorithm was applied. The crystal structure of BSA was taken from the Brookhaven Protein Data Bank (http:// www.rcsb.org/pdb) (PDB ID: 3 V03) (21). The Kollman charges were then assigned to the BSA structure and the geometry of SAD was optimized using the MM2 force field. Grid maps of $40 \times 40 \times 40$ points with a grid-point spacing of 0.3750 Å were generated using AutoGrid (22,23). LigPlot + was used to visualize the docked conformation and calculate the distances between possible hydrogen bonding partners (24). After 50 iterations, the most favorable docking model was selected according to the binding energy and geometry matching.

Results and discussion

The mechanism of fluorescence quenching

The UV/vis absorption spectra of BSA in the absence and presence of SAD were recorded and are presented in Fig. 1. It was observed that with gradual addition of SAD, the intensity of absorption spectra of BSA gradually increase at 278 nm. Furthermore, the absorption peak at 278 nm had an obvious red shift (~4 nm). This enhancement in the absorption of BSA in the presence of SAD and the red shift appear to be due to the formation of a ground state complex from the intermolecular interactions and the results exhibit a concentration-dependent relationship (25).

The effects of SAD on the fluorescence emission spectra of the BSA are shown in Fig. 2. In all cases, the fluorescence of BSA is gradually quenched along with the increase in SAD concentration, which can be illustrated by the interaction of SAD with BSA.

The fluorescence quenching mechanism can be classified into static quenching and dynamic quenching (26). To clarify the quenching mechanism between BSA and SAD, the Stern–Volmer equation was used to analyze the quenching data:

$$F_0/F = 1 + K_{SV}[Q] = 1 + k_q\tau_0[Q] \quad (2)$$

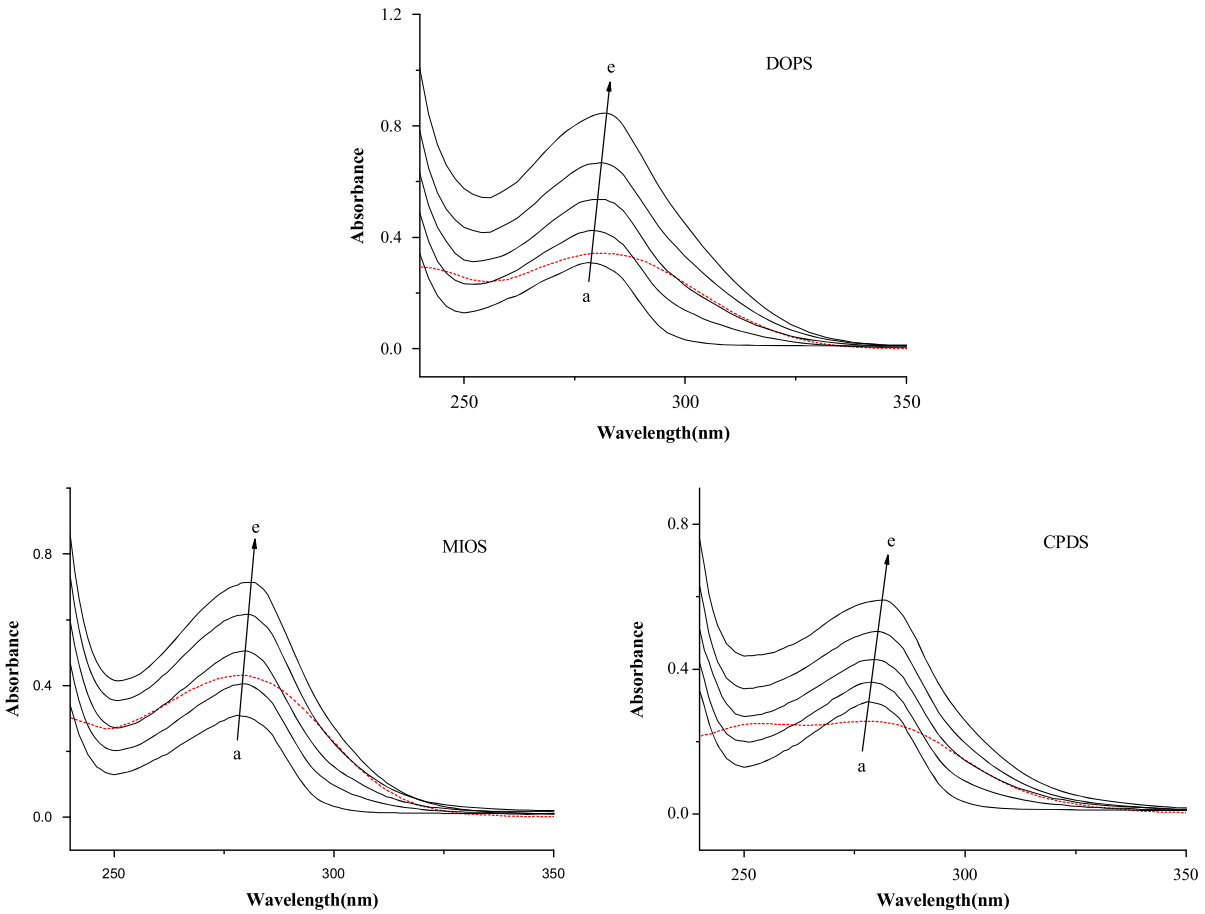

Figure 1. UV/vis absorption spectra of BSA in the presence of SAD at various concentrations. (a–e): c(BSA) = 1.00×10^{-5} mol/L; c(SAD) = 0.00, 0.50, 1.00, 1.50 and 2.00 ($\times 10^{-5}$ mol/L). The UV/vis absorption spectrum of SAD is represented by the red dotted curve, c(SAD) = 1.00×10^{-5} mol/L.

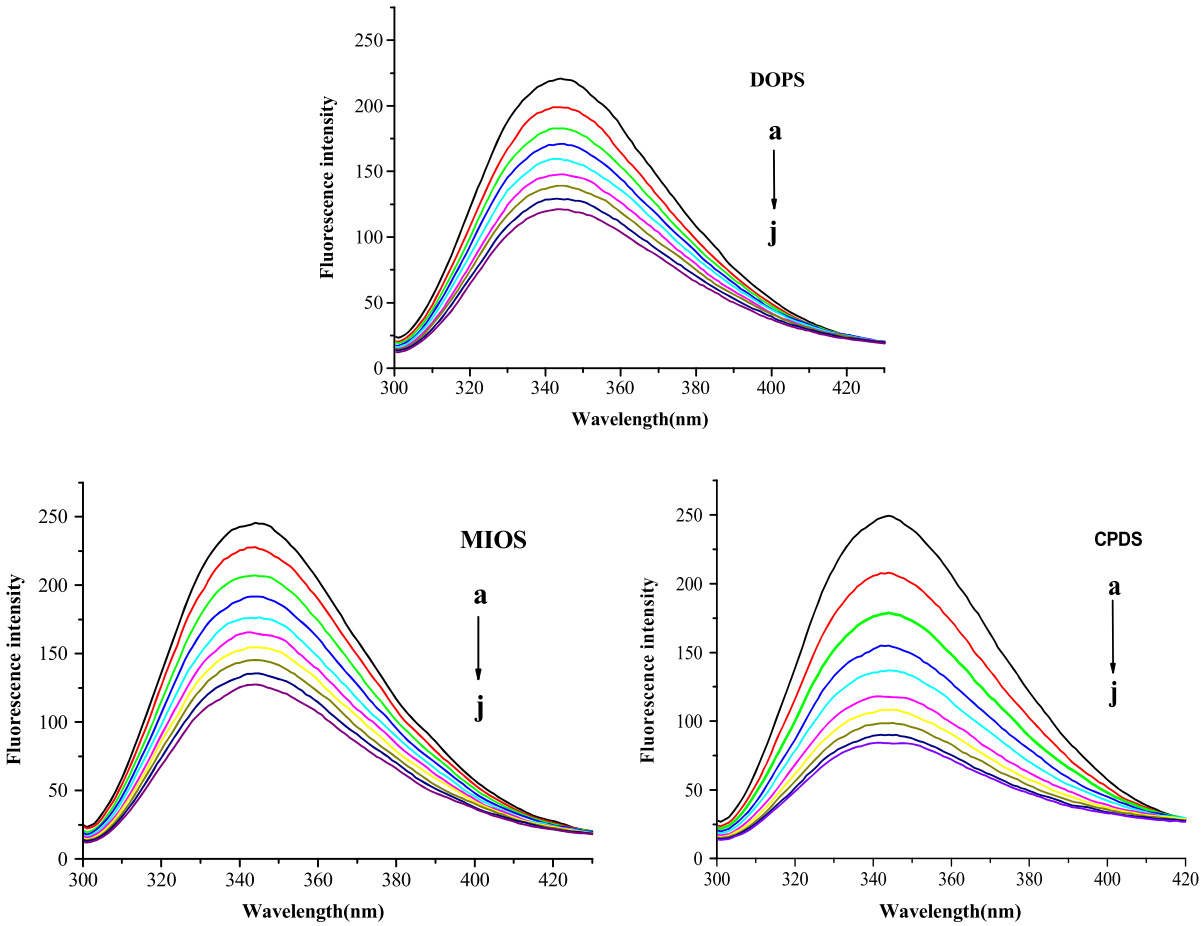

Figure 2. Fluorescence emission spectra of BSA in the presence of SAD at various concentrations and 304 K. λ_{ex} = 295 nm; *c* (BSA) =1.00 × 10^{-5} mol/L; from a to j, the concentration of DOPS, MIOS and CPDS was varied from 0 to 22.5 × 10^{-6} mol/L, in steps of 2.5 × 10^{-6} mol/L.

where F_0 and F are the steady-state fluorescence intensities in the absence and presence of SAD, respectively, k_q is the bimolecular quenching constant, τ_0 is the average lifetime of the biomolecule without the quencher and its value is considered to be 10^{-8} s, [*Q*] is the concentration of SAD and K_{SV} is the Stern–Volmer quenching constant (27).

The Stern–Volmer plots of the quenching of BSA fluorescence by SAD at different temperatures are displayed in Fig. 3. It can be seen that all Stern–Volmer plots exhibit a comparatively good linear relationship, suggesting that only one type of quenching occurs (28). The K_{SV} and k_q values calculated from the Stern–Volmer plots are listed in Table 1. The results show that all k_q values are apparently greater than the value of maximum diffusion collision quenching rate constant (2.00 × 10^{10} L/mol/s), which indicated that the fluorescence quenching mechanism of BSA–SAD at the investigated concentrations of SAD might be mainly governed by a static quenching rather than a dynamic quenching process (29).

To reconfirm that the probable fluorescence quenching mechanism of BSA–SAD was initiated by static quenching, the fluorescence lifetimes of BSA in the absence and presence of SAD were measured at room temperature. As seen in Table 2, the fluorescence lifetimes of BSA remain almost the same with the increase in SAD, which proves that the probable quenching mechanism of BSA–SAD is static quenching rather than dynamic quenching. In other words, the fluorescence quenching of BSA resulting from the complex formation is predominant (30).

The binding constant and binding sites

When small molecules bind independently to a set of equivalent sites on a macromolecule, the following equation can be used to determine the binding constant and the number of binding sites (31,32):

$$\log[(F_0 - F)/F] = \log\ K + n\log[Q] \quad (3)$$

where *K* is the binding constant and *n* is the number of binding sites between BSA and SAD. Figure 4 shows the linear fitting plots of log (F_0 – *F*)/*F* versus log [*Q*]. The values of *n* and *K*, listed in Table 3, can be calculated according to the slope and intercept of the double logarithm curve.

The *n* values are all 1, implying that there is one binding site between BSA and SAD. *K* values for BSA–DOPS, BSA–MIOS and BSA–CPDS are 4.864 × 10^4, 6.310 × 10^4 and 1.560 × 10^5 L/mol at 304 K, respectively, which indicates that there are stronger binding forces between BSA and SAD. As shown in Table 3, the binding constant of BSA–DOPS and BSA–MIOS decreased with the increase in temperature, at the same time, *n* is also inversely correlated with temperature, which shows that the binding of BSA with DOPS and MIOS is exothermic (33). However, the binding constant of BSA–CPDS and *n* increased with the increase in temperature, implying that the binding of BSA and CPDS is endothermic.

LUMINESCENCE
The Journal of Biological and Chemical Luminescence

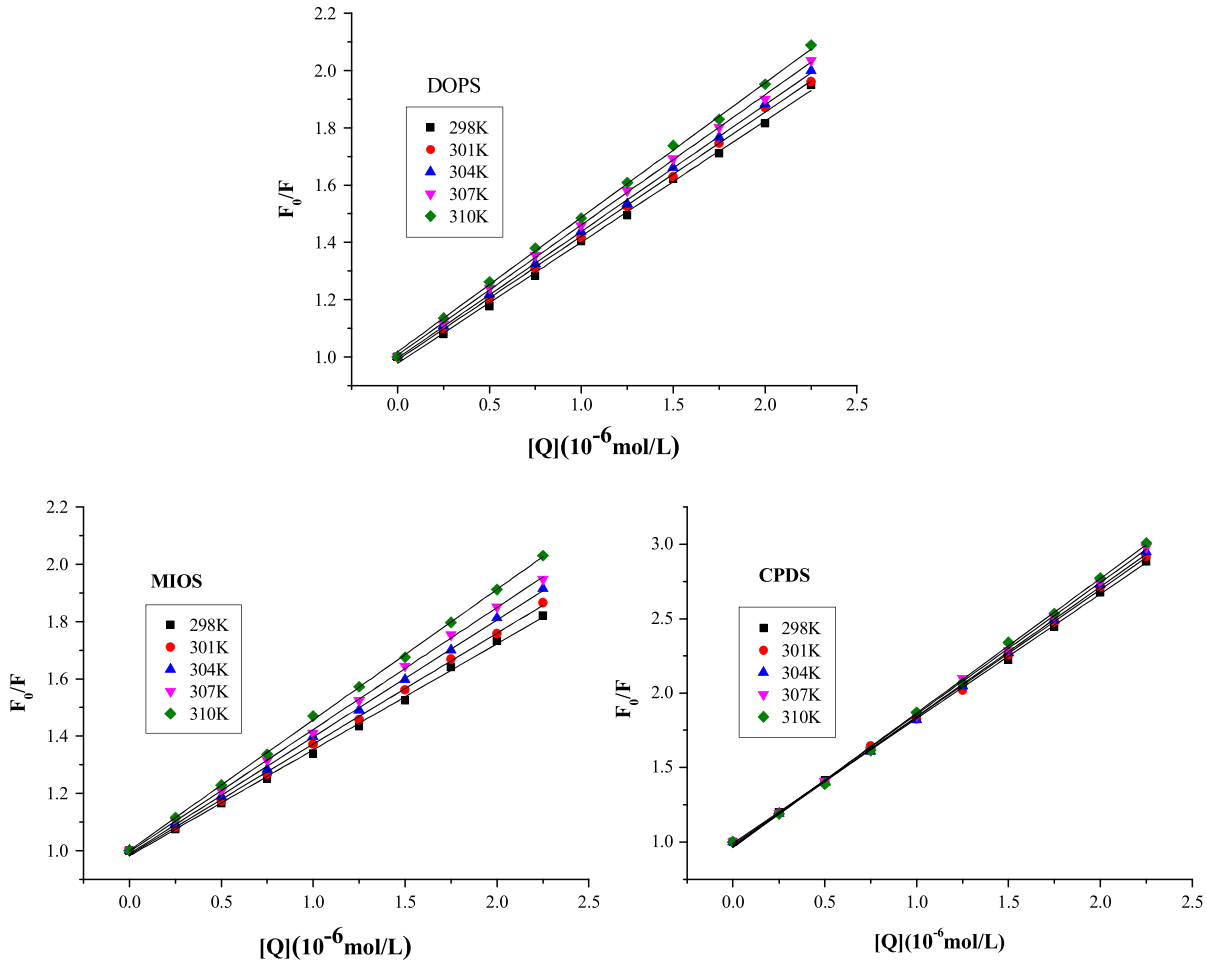

Figure 3. Stern–Volmer plots of BSA with SAD at different temperatures.

Table 1. Stern–Volmer quenching constants of BSA–SAD systems at 304 K

Compound	DOPS	MIOS	CPDS
*K*sv (L/mol)	4.428×10^5	4.087×10^5	8.729×10^5
k_q (L/mol/s)	4.428×10^{13}	4.087×10^{13}	8.729×10^{13}
R^2	0.9986	0.9988	0.9990

Table 2. Fluorescence lifetime of BSA in the presence of SAD

C_{SAD}/C_{BSA}	τ (ns)		
	DOPS	MIOS	CPDS
0.0	5.86	5.86	5.86
1.0	5.81	5.79	5.75
1.5	5.72	5.72	5.63
2.0	5.66	5.69	5.57

The acting force between BSA and SAD

In general, the acting forces between ligand and protein include hydrogen bonds, electrostatic forces, van der Waal's forces and hydrophobic forces. The thermodynamic parameters, enthalpy changes (ΔH) and entropy changes (ΔS), for the binding reaction are the main evidence used to confirm binding modes. From a thermodynamic standpoint, $\Delta H > 0$ and $\Delta S > 0$ suggest a hydrophobic interaction; $\Delta H < 0$ and $\Delta S < 0$ reflect van der Waal's forces or hydrogen bond formation; and $\Delta H \approx 0$ and $\Delta S > 0$ suggest an electrostatic force (34). To investigate the acting force between BSA and SAD, thermodynamic parameters dependent on the temperature, including the free energy change (ΔG), enthalpy change (ΔH) and entropy change (ΔS) were calculated on the basis of the van't Hoff equation:

$$\ln k = -\frac{\Delta H}{RT} + \frac{\Delta S}{R} \quad (4)$$

where K is the binding constant at the corresponding temperature, T is the experimental temperature and R is the gas constant. The fitted curve of ln$K$ against $1/T$ is shown in Fig. 5. The enthalpy change (ΔH) is calculated from the plot of ln$K$ versus $1/T$. The free energy change (ΔG) can be estimated from:

$$\Delta G = \Delta H - T\Delta S \quad (5)$$

The calculated results are given in Table 4. The negative sign for ΔG indicates that the binding process for BSA and SAD is spontaneous.

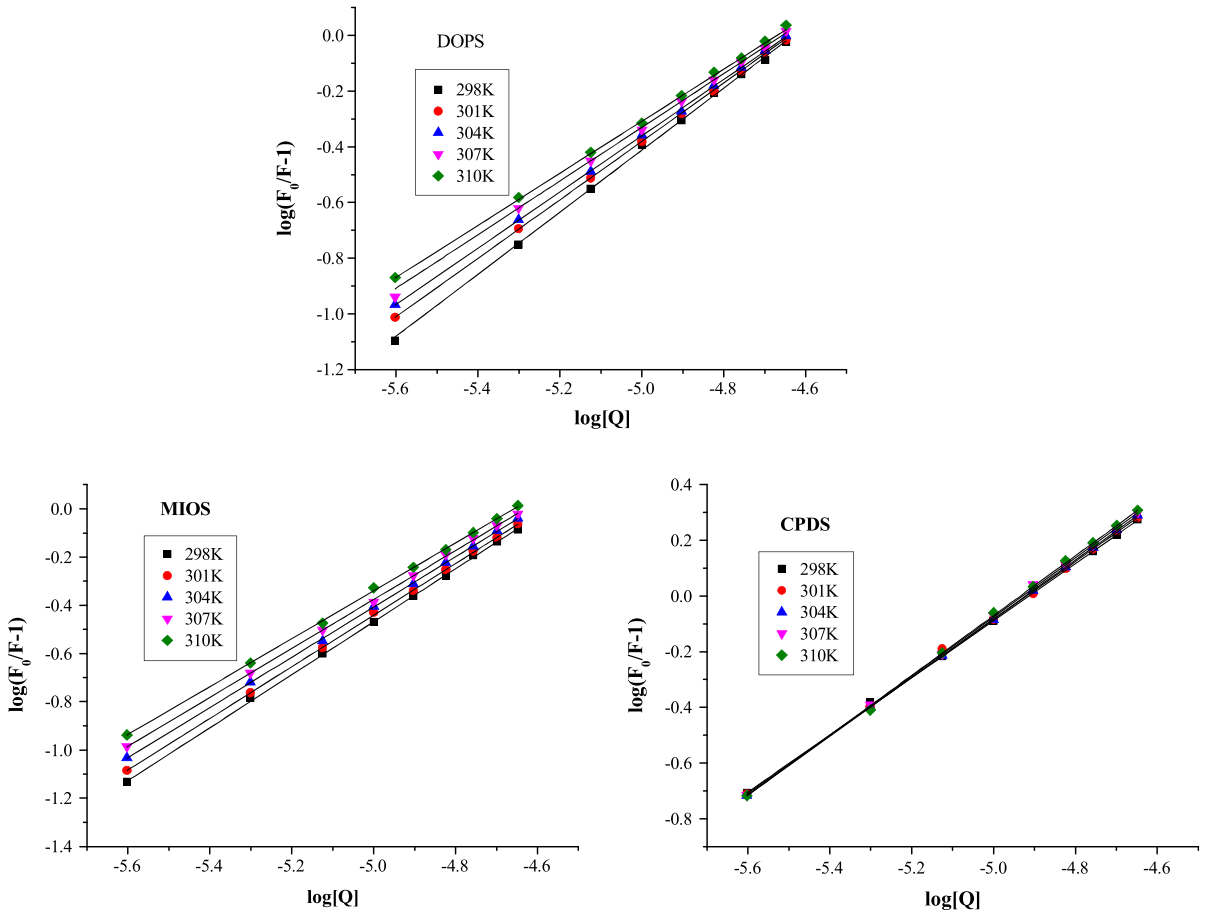

Figure 4. Double-log plots of BSA with SAD at different temperatures.

Table 3. Binding constants and binding sites of BSA–SAD systems

Compound	298 K		301 K		304 K		307 K		310 K	
	K (L/mol)	*n*	*K* (L/mol)	*n*	*K* (L/mol)	*n*	*K* (L/mol)	*n*	*K* (L/mol)	*n*
DOPS	1.428×10^5	1	7.362×10^4	1	4.864×10^4	1	3.090×10^4	1	2.317×10^4	1
MIOS	1.052×10^5	1	8.110×10^4	1	6.310×10^4	1	4.977×10^4	1	4.217×10^4	1
CPDS	1.099×10^5	1	1.315×10^5	1	1.560×10^5	1	1.742×10^5	1	2.014×10^5	1

The ΔH and ΔS values for BSA and two SADs (DOPS and MIOS) are negative, suggesting that the main acting forces between BSA and DOPS and MIOS are hydrogen bonds and van der Waal's forces. As for BSA–CPDS, the positive values of ΔH and ΔS mean that hydrophobic forces are the main acting forces between BSA and CPDS.

Energy transfer between BSA and sulfonamide derivatives

According to Förster non-radioactive energy transfer theory, the efficiency of energy transfer E and the binding distance r between the BSA and SAD can be calculated using following equation (35,36):

$$E = 1 - \frac{F}{F_0} = \frac{R_0^6}{R_0^6 + r^6} \tag{6}$$

where r is the binding distance between donor and acceptor, and R_0 is the critical distance when the efficiency (E) of energy transfer is 50%. The value of R_0 can be calculated from equation (7):

$$R_0^6 = 8.8\times10^{-25} K^2 \phi N^{-4} J \tag{7}$$

where the K^2 is the spatial orientation factor of the dipole, N is the refractive index of the medium, Φ is the fluorescence quantum yield of the donor in the absence of the acceptor and J is the overlap integral of the fluorescence emission spectrum of the donor and the absorption spectrum of the acceptor. In the present case, $K^2 = 2/3$, $N = 1.336$ and $\Phi = 0.15$ for BSA (37). J is given by the following equation:

$$J = \frac{\sum F(\lambda)\varepsilon(\lambda)\lambda^4 \Delta\lambda}{\sum F(\lambda)\Delta\lambda} \tag{8}$$

LUMINESCENCE
The Journal of Biological and Chemical Luminescence

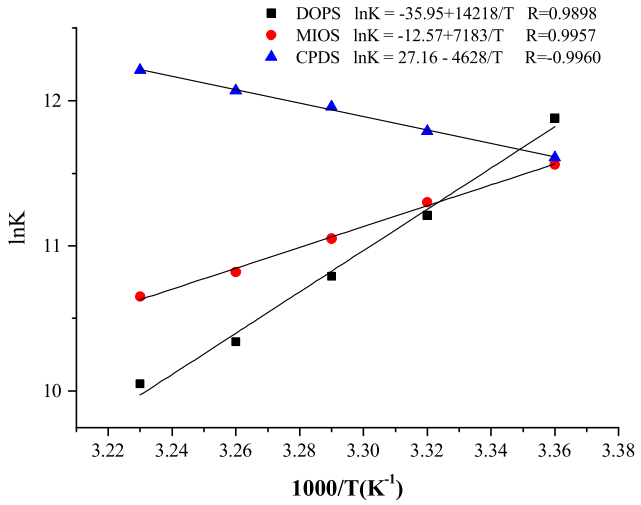

Figure 5. Van't Hoff plot of BSA with SAD.

where λ is the wavelength of the corresponding fluorescence spectrum of the BSA and the absorption spectrum of SAD. $F(\lambda)$ and $\varepsilon(\lambda)$ are the fluorescence intensity of the BSA and the molar absorption coefficient of SAD, respectively. Figure 6 shows the overlap between the fluorescence emission spectra of BSA and the absorption spectra of SAD at room temperature.

According to equations (6)–(8), J, E, R_0 and r can be calculated and the corresponding results are listed in Table 5. Obviously, the binding distances between BSA and SAD are lower than the 2–6 nm range over which long-range interactions such as energy transfer take place (28) and confirm that static quenching is taking place and the fluorescence quenching is a result of binding of BSA with SAD and not through an energy transfer process, which is also in accordance with a static quenching mechanism.

Conformation investigation

The synchronous fluorescence spectrum is a powerful tool to explore the microenvironment of amino acid residues by

Table 4. Thermodynamic parameters of BSA–SAD systems

Compound	ΔG (kJ/mol)					ΔH (kJ/mol)	ΔS (J/K/mol)
	298 K	301 K	304 K	307 K	310 K		
DOPS	−29.14	−28.24	−27.34	−26.45	−25.55	−118.21	−298.90
MIOS	−28.58	−28.26	−27.95	−27.63	−27.32	−59.72	−104.51
CPDS	−28.82	−29.50	−30.18	−30.85	−31.53	38.48	225.85

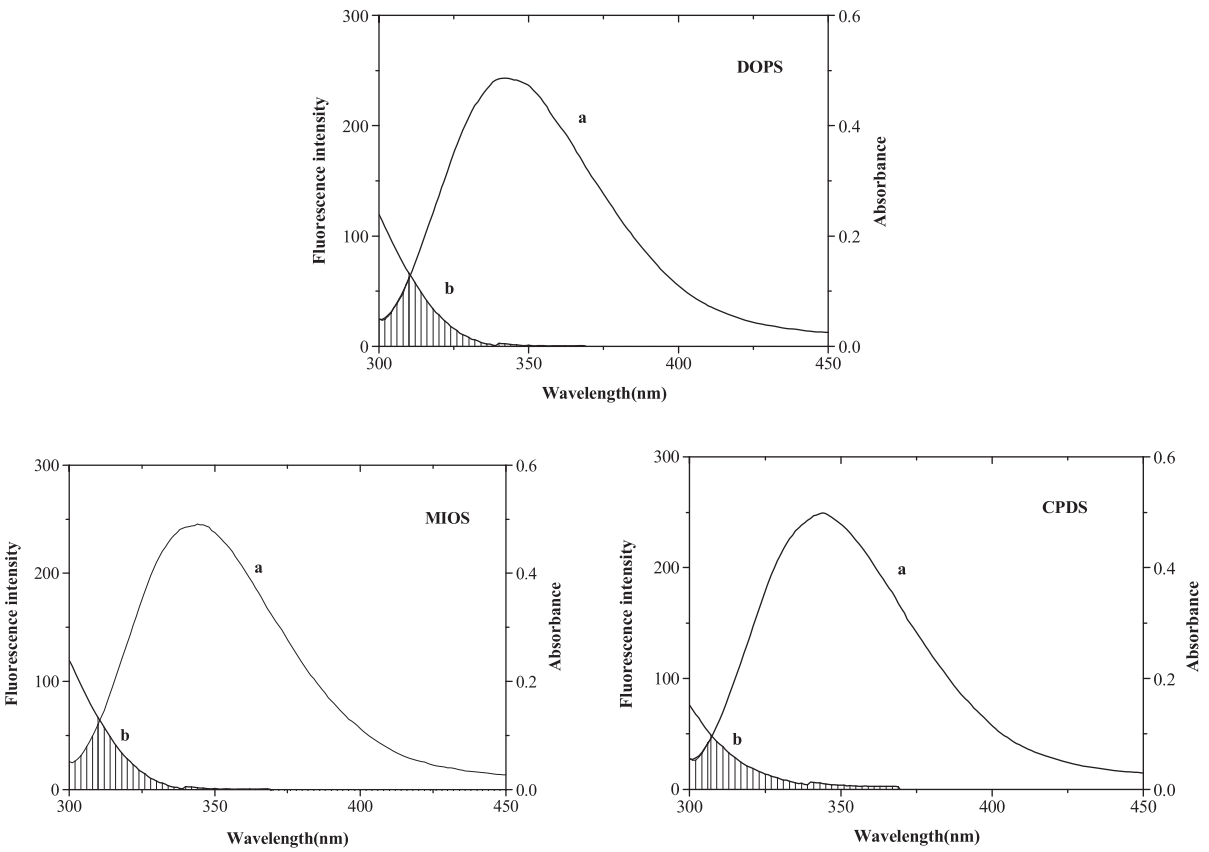

Figure 6. The overlap of the fluorescence emission spectrum of BSA (a) and the absorption spectrum of SAD (b). $c(\text{BSA}) = c(\text{SAD}) = 1.0 \times 10^{-5}$ mol/L.

Table 5. Energy transfer parameters of BSA-SAD systems

System	J (cm^3/L/mol)	R_0 (nm)	r (nm)	E
BSA–DOPS	1.16×10^{-15}	1.78	1.93	0.38
BSA–MIOS	1.01×10^{-15}	1.74	1.96	0.33
BSA–CPDS	1.29×10^{-15}	1.81	1.87	0.45

measuring the emission wavelength shift, because the shift in the position of maximum emission wavelength corresponds to changes in the polarity around the chromosphere molecule (38–40). When $\Delta\lambda$ between the excitation and emission wavelengths is stabilized at either 15 or 60 nm, the synchronous fluorescence spectrum can give the characteristics of tyrosine residues or tryptophan residues (41). The synchronous fluorescence spectra of the BSA–SAD system are shown in Fig. 7.

As shown in Fig. 7, the maximum emission wavelengths of tryptophan residues have no significant shift, which indicates that SAD has little effect on the microenvironment of tryptophan residues. The emission peaks of tyrosine residues show a slight red shift, suggesting that the hydrophobicity around tyrosine residues decreased and the polarity increased. Therefore, the microenvironment of tyrosine residues was

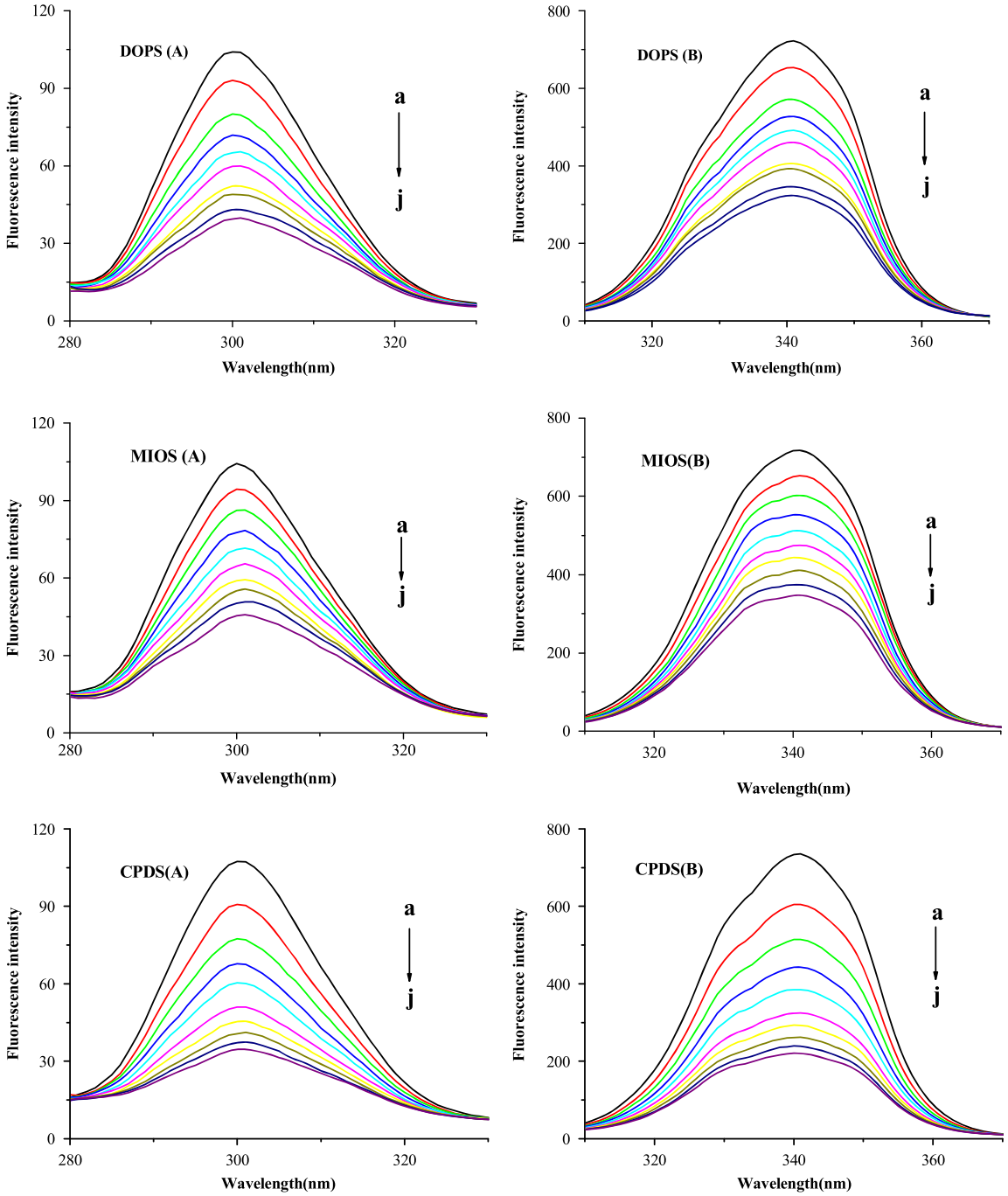

Figure 7. Synchronous fluorescence spectra of BSA with SAD. (A) $\Delta\lambda = 15$ nm, (B) $\Delta\lambda = 60$ nm; T = 304 K; c(BSA) = 1.00×10^{-5} mol/L; from a to j, the concentration of DOPS, MIOS and CPDS was varied from 0 to 22.5×10^{-6} mol/L, in steps of 2.5×10^{-6} mol/L.

LUMINESCENCE
The Journal of Biological and Chemical Luminescence

changed, resulting in conformational changes in BSA during the binding process.

Circular dichroism spectra

Circular dichroism (CD) spectroscopy is a sensitive technology to monitor the secondary structure alteration of protein. In order to further investigate the conformational changes, the CD spectra of BSA in the absence and presence of SAD were measured. The CD results were expressed in terms of mean residue ellipticity (MRE) in deg cm^2/dmol according to the following equation (19):

$$[\theta_\lambda] = \frac{\theta}{10nlc} \tag{9}$$

where c is the molar concentration of BSA, θ is the observed rotation in deg, n is the number of amino acid residues of protein (583 for BSA) and l is the path length (0.1 cm).

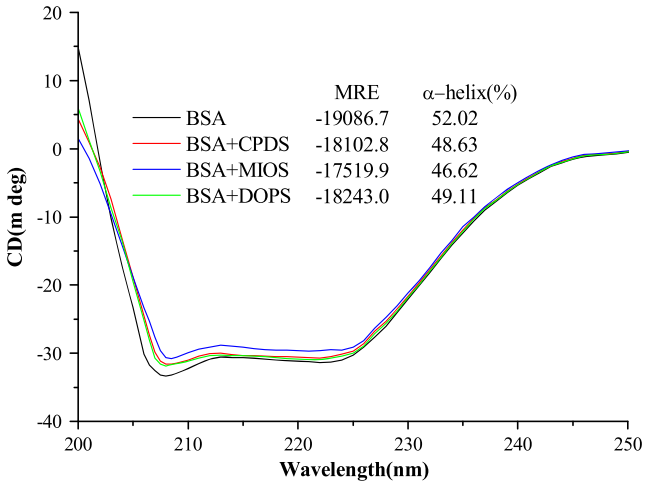

Figure 8. CD spectra of BSA with SAD. $c(BSA) = c(SAD) = 3.0 \times 10^{-6}$ mol/L.

The α-helix contents of BSA were calculated from MRE values at 208 nm using the following equation (19):

$$\alpha - helix(\%) = \frac{-[\theta]_{208} - 4000}{33000 - 4000} \tag{10}$$

where $[\theta]_{208}$ is the observed MRE value at 208 nm, 4000 is the MRE of the β form and random coil conformation cross at 208 nm, and 33 000 is the MRE value of a pure α helix at 208 nm.

The CD spectra of BSA–SAD complex are shown in Fig. 8. It was observed that SAD caused decrease in α-helix content, and MIOS led to the greatest change, whereas DOPS caused the least change. All the data confirm that the interaction between BSA and SAD leads to a change of the protein's secondary structure.

Molecular docking analysis

The binding mode of BSA and SAD are shown in Fig. 9. SAD was situated in subdomain IIA of BSA (Fig. 9a). The residue Trp213 was in close proximity to SAD (Fig. 9b), which provides a good structural basis to explain the fluorescence quenching of BSA in the presence of SAD. SAD were surrounded by hydrophobic side chains, suggesting that hydrophobic forces were the main interaction forces in the binding of BSA with SAD. Furthermore, hydrogen bonding was formed between BSA and SAD, and because of the presence of many polar and ionic amine acid residues near SAD, such as Arg194, Arg198, Arg217, Asp450, Lys294, Ser201 and Ser343, there were also a considerable number of hydrogen bonding and electrostatic interactions between BSA and SAD, which was supported by the thermodynamic analysis. For the complexes BSA–DOPS, BSA–MIOS and BSA–CPDS, the free energy change of binding (ΔG) obtained from the docking simulation were –27.17, –22.10 and –26.62 kJ/mol, respectively, which is less comparable with the experimental free energy of binding obtained from acting force study. This difference between experimental and theoretical results may be due

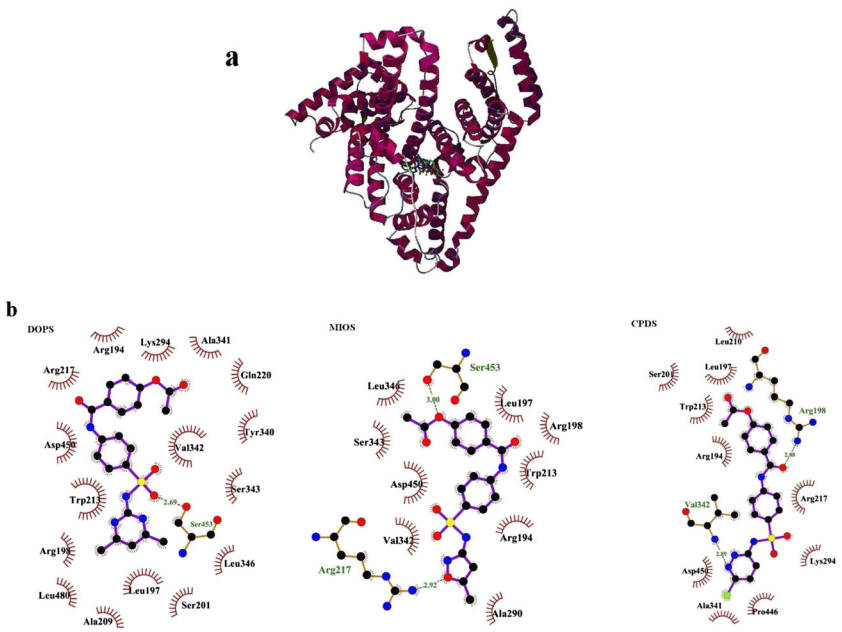

Figure 9. (a) The binding mode of BSA and SAD. Red, CPDS; blue, MIOS; green, DOPS. The BSA structure is displayed as a ribbon diagram, and SAD are shown with stick model. (b) Ligplot representations of the interactions between BSA and SAD. The hydrogen bondings are shown using green dashed line.

to exclusion of solvent in docking simulations or rigidity of the receptor other than tryptophan (42).

Conclusions

The interactions between BSA and SAD were investigated under simulated physiological conditions using a spectroscopic method. SAD can quench the fluorescence of BSA via a static quenching process, implying that BSA can bind with SAD and form a BSA–SAD complex. The large association constants and the shorter binding distances between BSA and SAD indicate that SAD can bind with BSA with high possibility. The microenvironment and conformation of BSA were changed slightly in the binding reaction based on analysis of the synchronous fluorescence and CD spectra. Molecular modeling results show that SAD was situated in subdomain IIA of BSA. These results will be helpful in understanding the pharmacodynamics and pharmacokinetics of related drugs.

Acknowledgments

The research was financially supported by the Natural Science Foundation of Guangxi Province (2011GXNSFA018051, 2013GXNSFDA019005).

References

1. Tan F, Guo M, Yu Q. Studies on interaction between gatifloxacin and human serum albumin as well as effect of copper(II) on the reaction. Spectrochim Acta A 2005;61:3006–12.
2. Figgie J, Rossing TH, Fencl V. The role of serum-proteins in acid–base equilibria. J Lab Clin Med 1991;117:453–67.
3. Mathias U, Jung M. Determination of drug–serum protein interactions via fluorescence polarization measurements. Anal Bioanal Chem 2007;388:1147–56.
4. Yu ZL, Li DJ, Ji BM, Chen JJ. Characterization of the binding of nevadensin to bovine serum albumin by optical spectroscopic technique. J Mol Struct 2008;889:422–8.
5. Rieutord A, Bourget P, Torché G, Zazzo JF. In vitro study of the protein binding of fusidic acid: a contribution to the comprehension of its pharmacokinetic behaviour. Int J Pharm 1995;119:57–64.
6. Flarakos J, Morand KL, Vouros P. high-throughput solution-based medicinal library screening against human serum albumin. Anal Chem 2005;77:1345–53.
7. Dockal M, Carter DC, Rüker F. Conformational transitions of the three recombinant domains of human serum albumin depending on pH. J Biol Chem 2000;275:3042–50.
8. Carter DC, Chang B, Ho JX, Keeling K, Krishnasami Z. Preliminary crystallographic studies of four crystal forms of serum albumin. Eur J Biochem 1994;226:1049–52.
9. El-Sayed NS, El-Bendary ER, El-Ashry SM, El-Kerdawy MM. Synthesis and antitumor activity of new sulfonamide derivatives of thiadiazolo[3,2-*a*]pyrimidines. Eur J Med Chem 2011;46:3714–20.
10. Nuria PN, Ester GI, Ángel M, Rosa P. Development of a group-specific immunoassay for sulfonamides: application to bee honey analysis. Talanta 2007;71:923–33.
11. Silke MF, Peter E. Sulfonamides in dermatology. Clin Dermatol 2003;21:7–11.
12. Rice-Evans CA, Miller NJ, Pagana G. Structure–antioxidant activity relationships of flavonoids and phenolic acids. Free Radical Biol Med 1996;20:933–56.
13. Huang MT, Smart RC, Wong CQ, Conney AH. Inhibitory effect of curcumin, chlorogenic acid, caffeic acid, and ferulic acid on tumor promotion in mouse skin by 12-*o*-tetradecanoylphorbol-13-acetate. Cancer Res 1988;48:5941–6.
14. Arimoto S, Inada N, Rai H, Nakano H, Negishi T, Hayatsu H. Effect of chlorophyllin sulfonamide derivatives on the mutagenicity of 3-hydroxyamino-1-methyl-5*H*-pyrido-[4,3-*b*]indole, Trp-P-2(NHOH). Mutat Res 1991;253:242.
15. Vennat B, Pourrat A, Pourrat H, Gross D, Bastide P, Bastide J. Procyanidins from the roots of *Fragaria vesca*: characterization and pharmacological approach. Chem Pharm Bull 1988;36:828–33.
16. Isik K, Özdemir-Kocak F. Antimicrobial activity screening of some sulfonamide derivatives on some *Nocardia* species and isolates. Microbiol Res 2009;164:49–58.
17. Lima LM, Ormelli CB, Brito FF, Miranda AL, Fraga CA, Barreiro EJ. Synthesis and antiplatelet evaluation of novel aryl-sulfonamide derivatives, from natural safrole. Pharm Acta Helv 1999;73:281–92.
18. Özdemir ÜÖ, Güvenç P, Şahin E, Hamurcu F. Synthesis, characterization and antibacterial activity of new sulfonamide derivatives and their nickel(II), cobalt(II) complexes. Inorg Chim Acta 2009;362: 2613–8.
19. Mandal G, Bardhan M, Ganguly T. Occurrence of Förster resonance energy transfer between quantum dots and gold nanoparticles in the presence of a biomolecule. J Phys Chem C 2011;115: 20840–8.
20. Morris GM, Goodsell DS, Halliday RS, Huey R, Hart WE, Belew RK, et al. Automated docking using a Lamarckian genetic algorithm and an empirical binding free energy function. J Comput Chem 1998; 19:1639–62.
21. Bujacz A. Structures of bovine, equine and leporine serum albumin. Acta Crystallogr D 2012;68:1278–89.
22. Sanner MF. Python: a programming language for software integration and development. J Mol Graph Model 1999;17:57–61.
23. Trott O, Olson AJ. AutoDock Vina: improving the speed and accuracy of docking with a new scoring function, efficient optimization, and multithreading. J Comput Chem 2010;31:455–61.
24. Laskowski RA, Swindells MB. LigPlot+: multiple ligand–protein interaction diagrams for drug discovery. J Chem Inf Model 2011;51: 2778–86.
25. Bardhan M, Misra T, Ganguly T. Quantization of bovine serum albumin by fluorescence enhancement effects and corresponding binding of macrocyclic host–protein assembly. J Photochem Photobiol B 2012;106:113–9.
26. Papadopoulou A, Green R J, Frazier RA. Interaction of flavonoids with bovine serum albumin: a fluorescence quenching study. J Agric Food Chem 2005;53:158–63.
27. Lakowicz JR, Weber G. Quenching of fluorescence by oxygen. Probe for structural fluctuations in macromolecules. Biochemistry 1973;12: 4161–70.
28. Lakowicz JR. *Principles of fluorescence spectroscopy*. 3rd ed. New York: Springer, 2006.
29. Zhang YP, Shi SY, Peng MJ. Investigation of proton pump inhibitors binding with bovine serum albumin and their relationship to molecular structure. J Lumin 2012;132:1921–8.
30. Wang J, Guo YW, Liu B, Cheng CP, Wang ZQ, Han GX, et al. Spectroscopic analyses on interaction of bovine serum albumin (BSA) with toluidine blue (TB) and its sonodynamic damage under ultrasonic irradiation. J Lumin 2011;131:231–7.
31. Zhao HW, Ge M, Zhang ZX, Wang WF, Wu GZ. Spectroscopic studies on the interaction between riboflavin and albumins. Spectrochim Acta A 2006;65:811–7.
32. Yu XY, Lu SY, Yang Y, Li XF, Yi PG. Study on the interaction between NCP-(4-hydroxycoumarins) and bovine serum albumin by spectroscopic techniques. Spectrochim Acta A 2012;91:113–7.
33. Machicote RG, Pacheco ME, Bruzzone L. Binding of several benzodiazepines to bovine serum albumin: fluorescence study. Spectrochim Acta A 2010;77:466–72.
34. Ross PD, Subramanian S. Thermodynamics of protein association reactions: forces contributing to stability. Biochemistry 1981;20: 3096–102.
35. Meng FY, Zhu JM, Zhao AR, Yu SR, Lin CW. Synthesis of *p*-hydroxycinnamic acid sulfonamide derivatives and investigation of fluorescence binding with bovine serum albumin. J Lumin 2012;132:1290–8.
36. He LL, Wang X, Liu B, Wang J, Sun YG. interaction between ranitidine hydrochloride and bovine serum albumin in aqueous solution. J Solution Chem 2010; 39:654–64.
37. Hua YJ, Liu Y, Wang JB, Xiao XH, Qua SS. Study of the interaction between monoammonium glycyrrhizinate and bovine serum albumin. J Pharm Biomed Anal 2004;36:915–9.
38. Bi SY, Song DQ, Tian Y, Zhou X, Liu ZY, Zhang HQ. Molecular spectroscopic study on the interaction of tetracyclines with serum albumins. Spectrochim Acta A 2005;61:629–36.

LUMINESCENCE
The Journal of Biological and Chemical Luminescence

39. Yuan T, Weljie AM, Vogel HJ. Tryptophan fluorescence quenching by methionine and selenomethionine residues of calmodulin: orientation of peptide and protein binding. Biochemistry 1998;37: 3187–95.
40. Shi YJ, Liu HY, Xu M, Li ZP, Xie GQ, Huang L, et al. Spectroscopic studies on the interaction between an anticancer drug ampelopsin and bovine serum albumin. Spectrochim Acta A 2012;87: 251–7.
41. Pan XR, Liu RT, Qin PF, Wang L, Zhao XC. Spectroscopic studies on the interaction of acid yellow with bovine serum albumin. J Lumin 2010;130:611–7.
42. Jana S, Dalapati S, Ghosh S, Guchhait N. Binding interaction between plasma protein bovine serum albumin and flexible charge transfer fluorophore: a spectroscopic study in combination with molecular docking and molecular dynamics simulation. J Photochem Photobiol A 2012;231:19–27.